Interaction between Shocks and Clumps With Self-Contained Magnetic Fields

Shule Li[a,*], Adam Frank[a], Eric G. Blackman[a]

[a] *Department of Physics and Astronomy, University of Rochester, Rochester, NY, 14627*

Abstract

Problems involving magnetized clouds and clumps, especially their interaction with shocks are common in astrophysical environments and have been a topic of research in the past decade. Many previous numerical studies have focused on the problem of clumps immersed in a globally uniform magnetic field subject to a oncoming shock. However, realistic clumps may have tangled magnetic field self contained within them. This magnetic field will be compressed by the shock and its energy spectrum and spatial structure may affect the evolution of the clump during the shock encounter. Using our parallel MHD code AstroBEAR, we set up an initial state with magnetized clumps of different contained magnetic field configurations. We then drive strong shocks through these clumps (including the effects of radiative cooling) and compare our results to previous studies of global uniform field scenarios.

Keywords: magneto-hydrodynamics, planetary nebula, radiative shocks, MHD clumps, MHD jets

1. Introduction

The problem of clumps interacting with shocks is important for understanding how the interstellar medium interacts with supernova remnants and other clumpy outflows. Magnetic fields are present in such an interaction and thus their effect is important to consider. Most previous numerical studies focus on clumps immersed in a uniform background magnetic field [1] [2].

Early analytic studies of single clump/shock interaction focused on the early stages of the hydrodynamic interaction, where the solution remained amendable to linear approximations. The evolution late in time, when the behavior becomes highly nonlinear, remains intractable from a purely analytic standpoint and therefore has benefited greatly from numerical investigation – a review of the pioneering literature may be found in the work of Klein, McKee and Colella [3] (hereafter KMC94), or Poludnenko et al [4]. Illustrating the maturity of the

*Corresponding author
Email address: shuleli@pas.rochester.edu (Shule Li)

field, a variety of physics has now been included in the studies. KMC94 discussed systematically the evolution of a single, adiabatic, non-magnetized, non-thermally conducting shocked clump overrun by a planar shock in axisymmetry ("2.5D"). Similar simulations were carried out in three dimensions (3-D) [5]. The role of radiative cooling [6] [7], smooth cloud boundaries [8], and systems of clumps [4] have all been studied. A similar problem involving clump-clump collisions, has also received attention [9] [10]. Most studies predominantly use an Eulerian mesh with a single- or two-fluid method to solve the inviscid Euler equations. One notable exception is Pittard's work [11], who use a "$\kappa-\epsilon$" model to explicitly handle the turbulent viscosity.

Through these studies, it is clear that: (1) When the field is parallel to the shock normal, the magnetic field is amplified at the front of and behind the clump. The front of the shocked clump is streamlined but there is no significant suppression on the fragmentation of the clump even for low initial magnetic β (where β is the ratio of thermal to magnetic pressure). (2) When the magnetic field is perpendicular to the shock normal, the field wraps around the clump and gets greatly amplified due to stretching. The shocked clump is highly streamlined and the fragmentation can be greatly suppressed even for high initial β. Adding radiative cooling leads to thinner fragments and confined boundary flows [12]. There are also studies in recent years focusing on the multi-physics of the problem by incorporating thermal diffusion [13].

In reality, clump formation may result in magnetic fields self-contained within a clump which is not well modeled by assuming the clumps are immersed in a uniform background field: If a cold shell embeded in a hot environment evolves towards thermal equilibrium by thermal conduction and the shell contains a tangeld field, some of the shell material will be captured and a tangled field can disconnect from the background field as the thermal conduction is anisotropic. This can form clumps with an internal magnetic field [14].

The purpose of this paper is to include internal magnetic fields in shock-clump interaction simulations for the first time. We assume that the contained magnetic field has a well defined geometric structure, and show that the shocked behavior of the clump indeed depends on the contained field even if the field is not enegetically dominant compared to the shock.

2. Numerical Method

For the simulations we employed the AstroBEAR code using a 3-D computational grid. The AstroBEAR code is a parallel AMR Eulerian hydrodynamics code with capabilities for MHD in two- and three-dimensions. There are several schemes of varying order available for the user. Details on AstroBEAR may be found in [15] [16] and at https://clover.pas.rochester.edu/trac/astrobear. While the code can treat multiple atomic, ionic and molecular species, in this work we use third order accurate piecewise parabolic method with HLL Riemann solver. We assume the gas is composed of pure hydrogen. In our simulations, we implement the Dalgarno McCray cooling table as it is more realistic comparing

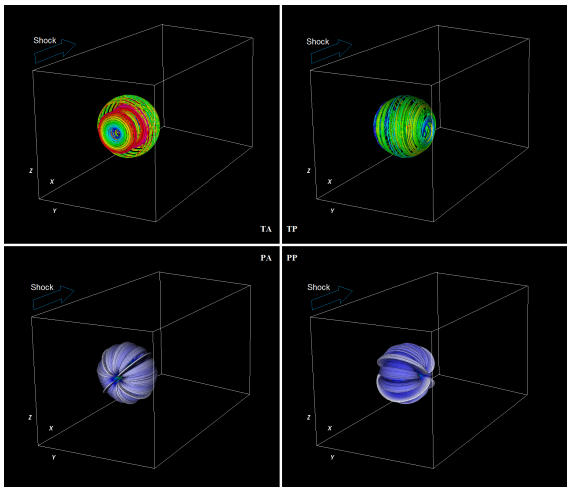

Figure 1: The initial setup of the clump simulations. The actual domain is four times as long on x as on y and z. The upcoming planar shock is at the left face of the domain, propagating rightward along the x axis. The streamlines show magnetic field orientations. The field configurations are labeled "TA", "TP", "PA" and "PP" corresponding to Tab.1.

to simple analytic cooling functions [17]. The gas is allowed to cool to a floor temperature of $50K$ and then cooling is turned off.

The resistivity is ignored in our calculation so that the dissipation of the magnetic field is numerical only. Small artificial viscosity and diffusion are implemented in order to achieve required stability and symmetry and prevent carbuncles which can occur when strong cooling and shocks are coupled. AstroBEAR has shown excellent scaling up to 10^4 processors [16] and the simulations presented in this paper were carried out on 1024 cores of an IBM Bluegene P machine at the University of Rochester's Center for Intergrated Computational Research. In the simulations presented here numerical considerations with the BlueGene machine led us to turn off AMR though we carried forward AMR versions of the runs on other machines.

3. Problem Description and Simlation Setup

The series of simulations presented in this paper are based on the same initial conditions for all quantities except the initial internal magnetic field of the clump to be shocked. The initial condition is illustrated by Fig.1. The domain is a box with dimensions $2400a.u. \times 60a.u. \times 60a.u.$ (the bounding box in Fig.1 does not represent the entire domain), with resolution $1440 \times 360 \times 360$, and open boundary conditions on the six sides of the box.

The ambient gas is non-magnetized and isothermal, with a particle number density of $1cc^{-1}$ and temperature of 10^4 K. A clump with radius of $r_c = 150a.u.$ is in thermal pressure equilibrium with the ambient medium. The clump has a density contrast of $\chi = 100$, i.e., particle number density of $100cc^{-1}$ and a

temperature of 100 K . It also contains an internal magnetic field with a peak magnetic induction of $30.88\mu G$. We define β_{min} and β_{avg} as the minimum ratio of thermal pressure to magnetic pressure and the ratio of thermal pressure to averaged magnetic pressure inside the clump, respectively:

$$\beta_{min} = \frac{P_{thermal}}{P_{B,peak}} \tag{1}$$

$$\beta_{avg} = \frac{P_{thermal}}{P_{B,avg}} \tag{2}$$

where $P_{B,peak}$ and $P_{B,avg}$ denote the peak and average magnetic field pressure respectively. In our simulations, we focus on the cases when the contained magnetic field is either purely poloidal or purely toroidal. Since poloidal and toroidal field configurations are different, the same peak magnetic pressure may yield different average magnetic field pressure. We have conducted numerical simulations for toroidal and poloidal contained field cases with $\beta_{avg} = 0.25$ and 1, respectively. The small value of β indicates that the clump is magnetic dominated. In this paper, we will be focusing on those simulations with $\beta_{avg} = 0.25$.

Since the magnetic field is not in a force free state, the clump will be deformed by the contained field at the time scale of:

$$\tau_{mag} = \frac{r_c}{u_A} \approx 276yrs \tag{3}$$

where u_A is the Alfvén speed of the contained field calculated from the average magnetic energy density inside the clump.

The geometrical configuration of the toroidal contained magnetic field (depicted in Fig.1) is best demonstrated using a cylindrical coordinates. Its mathematical expression is as follows:

$$B_r = 0 \tag{4}$$

$$B_\theta = \begin{cases} B_{0,tor}\frac{r}{fr_c}, & \text{if } r \le f\sqrt{r_c^2 - z^2} \\ B_{0,tor}\frac{\sqrt{r_c^2-z^2}-r}{(1-f)r_c}, & \text{if } r > f\sqrt{r_c^2 - z^2} \end{cases} \tag{5}$$

$$B_z = 0 \tag{6}$$

where r_c is the cut-off clump radius. For any given z, the magnetic field intensity peaks at $f\sqrt{r_c^2 - z^2}$. If f is close to 1, the field will be concentrated near the outer edge of the clump. In the presented simulations, we take $f = 0.9$.

The poloidal field is best demonstrated using the spherical coordinates. The magnetic field can be expressed as:

$$\mathbf{B_r} = 0 \tag{7}$$

$$\mathbf{B}_\theta = 0 \tag{8}$$

Table 1: Simulation Setups

Code	β_{avg}	Field Configuration	Field Orientation (related to shock)
TA	0.1	*toroidal*	aligned
TP	0.1	*toroidal*	perpendicular
PA	1	*poloidal*	aligned
PP	1	*poloidal*	perpendicular

$$\mathbf{B}_\phi = -\frac{B_{0,pol}(r_c - r)(r_c - 3r)sin\theta}{r_c} \tag{9}$$

We observe that the magnetic field energy density $\mathbf{B}^2$ peaks at the center $r = 0$ and has a weaker secondary maximum at $r = 2r_c/3$. The field attenuates to zero at the outer edge of the clump $r = r_c$. There is another zero point in between $r = 0$ and $r = r_c$: $r = r_c/3$. The toroidal and poloidal field setup are orthogonal to each other, and can be combined into a more general self-contained magnetic field distribution. The cases presented in our paper form the basis to understand more complex self-contained magnetic field configurations.

The incoming shock has a temperature of 10^6 K and Mach number $M = 10$ (where M is the ratio of the shock speed to the ambient sound speed). We identify the clump crushing time scale as:

$$\tau_{cc} = \frac{\sqrt{\chi}r_c}{u_{wind}} \approx 95yrs \tag{10}$$

The shock temperature is chosen so that the cooling time scale for the bow shock τ_{bow} is well below the clump crushing time to ensure effective cooling:

$$\tau_{bow} \approx 48yrs \ll \tau_{cc} \tag{11}$$

We also define the σ parameters of the shock: $\sigma_{thermal} = K_{shock}/E_{thermal}$ and $\sigma_{mag} = K_{shock}/E_{mag}$ as the ratio between the kinetic energy density of the shock and the thermal or average magnetic energy density contained in the clump, respectively.

From the previously given parameters, we can determine that $\sigma_{thermal} \approx 222$ and $\sigma_{mag} \approx 33$. Therefore, although the clump is magnetically dominated, the shock is much more energetic than either thermal or magnetic energy contained inside the clump. We run the simulation from time $t = 0$ to time $t \approx 333yrs$, i.e. $3.5\tau_{cc}$. We will use the clump crushing time τ_{cc} as our unit of time throughout the rest of the paper.

We study the shock-clump interactions when the clump contains an ordered magnetic field by running the simulations described in the following table:

4. Simulation Results

Fig.2 shows the result of a simulation with a shocked clump when the internal magnetic field is a toroidal and is aligned with the shock propagation direction

(coded TA in the previous section). Panels from top to bottom correspond to different evolution times: τ_{cc}, $2\tau_{cc}$ and $3.5\tau_{cc}$. The clump morphology is similar to that of the unmagnetized case (not shown) at τ_{cc}.At $2\tau_{cc}$, however, instead of being eroded by the RT instability and expanding, the clump material continues to collapse towards the symmetry axis due to the pinch by the toroidal magnetic field. Because of this compression, the flow driven off the clump does not fill the downstream domain with turbulence, but rather remains concentrated into a conical region. This trend continues at $3.5\tau_{cc}$, the clump material has become compressed into a very narrow cone with the toroidal field tightly wrapping around it. This geometry prevents the clump material from mixing with the ambient wind. The final snapshot resembles a "nose cone" observed in the MHD jet simulations [18] [19], with a small Mach angle.

In the case when the toroidal axis is perpendicular to the shock propagation direction, shown in Fig.3 (coded TP), the field pinches the clump onto z axis, but the shock compresses the clump onto the x axis. The result is a difference in aerodynamical resistance to the shock compression: the magnetized clump is harder to compress along z axis than x axis. As a result, the clump becomes football shaped at τ_{cc}. The oblate clump continues to be eroded by the incoming wind; at $2\tau_{cc}$, the clump begins to fragment mostly along the z axis because of a lack of compression by shock or field pinch. There is a ring-like feature that arises because the clump edge has a stronger field than the center. At the end of the simulation, the clump fragments along the z axis from erosion and cooling, and evolves to an array of cold, magnetized "clumplets".

Fig.4 shows the simulation of a shocked clump when the internal field is poloidal and aligned with the the shock normal (coded PA). In this case, there is a strong field concentration at the clump axis, as well as a relatively weak field at the clump surface. When the axis is aligned with the shock, we can see that during the compression phase, at τ_{cc}, the clump is compressed radially as in the unmagnetized case. Then, at $2\tau_{cc}$, we see a different form of evolution compared to previous cases. While the clump expands as in the unmagnetized case, it then develops a hollow core, the outer regions corresponding the domains with strong field. The regions with a weak initial field get distorted and compressed while the regions with a strong field better resist the compression. The "shaft" shaped feature surrounded by the hollow core has a relatively low β compared to the rest of the clump. It gradually deforms as a result of field pinching (squeezing here outwards from the axis) at the time scale of τ_{mag}, which is about $2.8\tau_{cc}$. Consequently, at $3.5\tau_{cc}$, the "shaft" disappears and the clump is fragmented into an array of cold, magnetized "clumplets", similar to the TP case.

Fig.5 shows the simulation with an internal poloidal field oriented perpendicular to the shock normal (coded PP). The influence of this different field orientation is evident at $t = 2\tau_{cc}$. Here the field concentration also produces a "shaft" and a "ring" as in the PA case, but both the "ring" and the "shaft" are partially eroded by the incoming shock. The "shaft" is then fragmented by the shock rather than the field pinch, and the "ring" leaves an extended **U**-shape. As a result, two large clumplets located on the y-z plane form at $3.5\tau_{cc}$.

Notice that the four previous cases all have unique downstream features: In

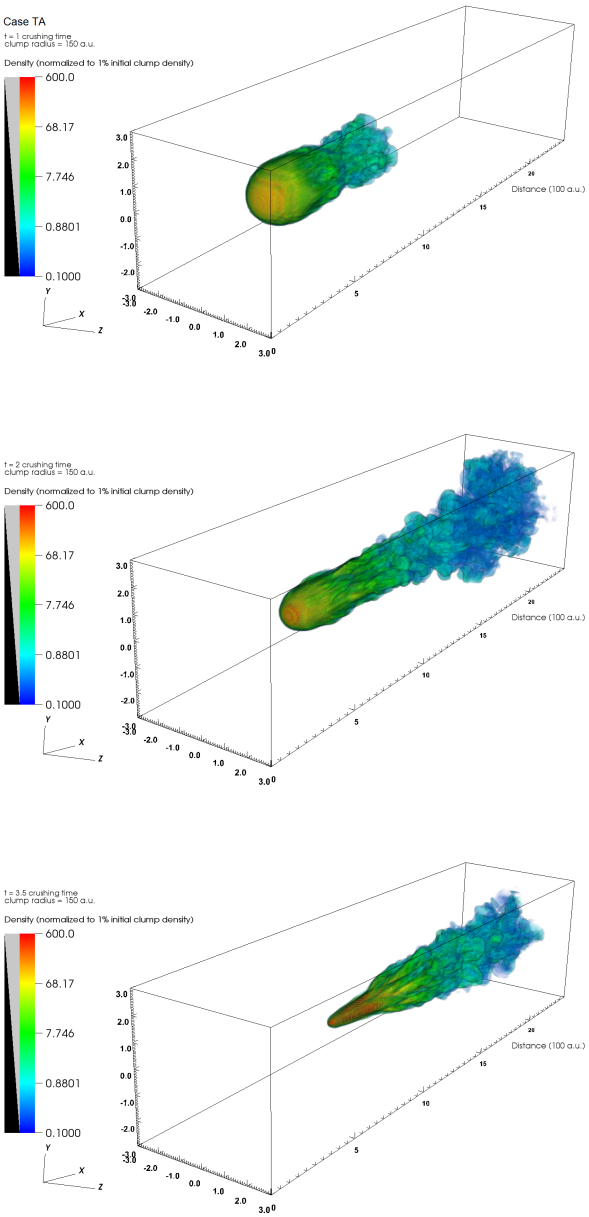

Figure 2: Case of toroidal field only, aligned with shock propagation direction (coded TA). Evolution of clump material at 1, 2 and 3.5 clump crushing times. The color indicates clump material concentration, normalized by initial value.

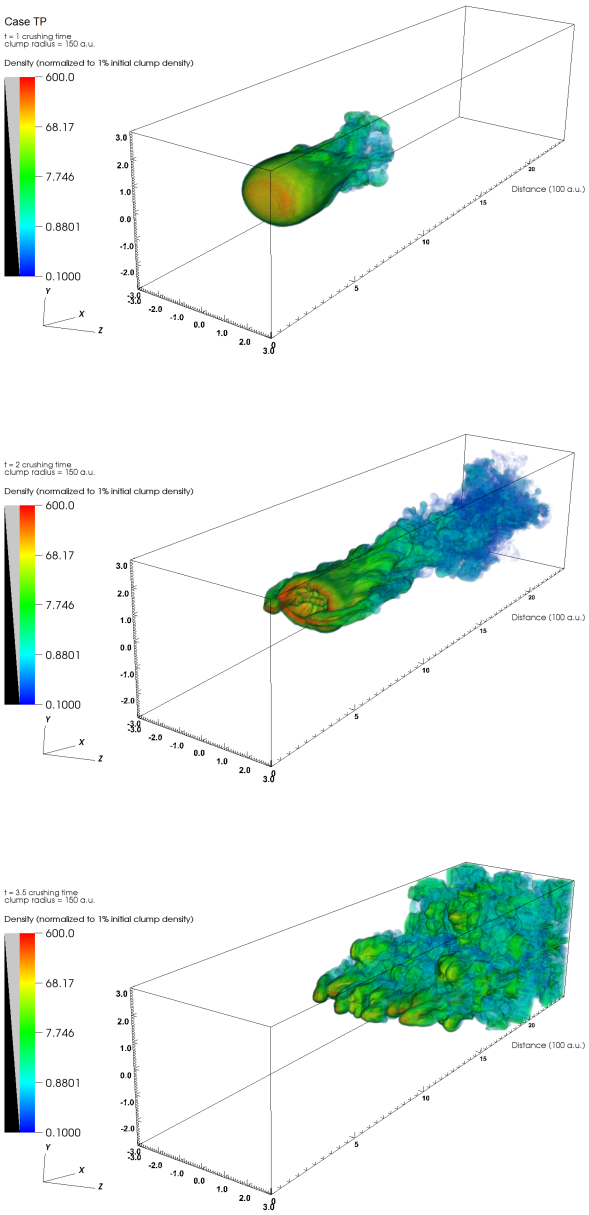

Figure 3: Case of toroidal field only, perpendicular to shock propagation direction (coded TP). Evolution of clump material at 1, 2 and 3.5 clump crushing times. The color indicates clump material concentration, normalized by initial value.

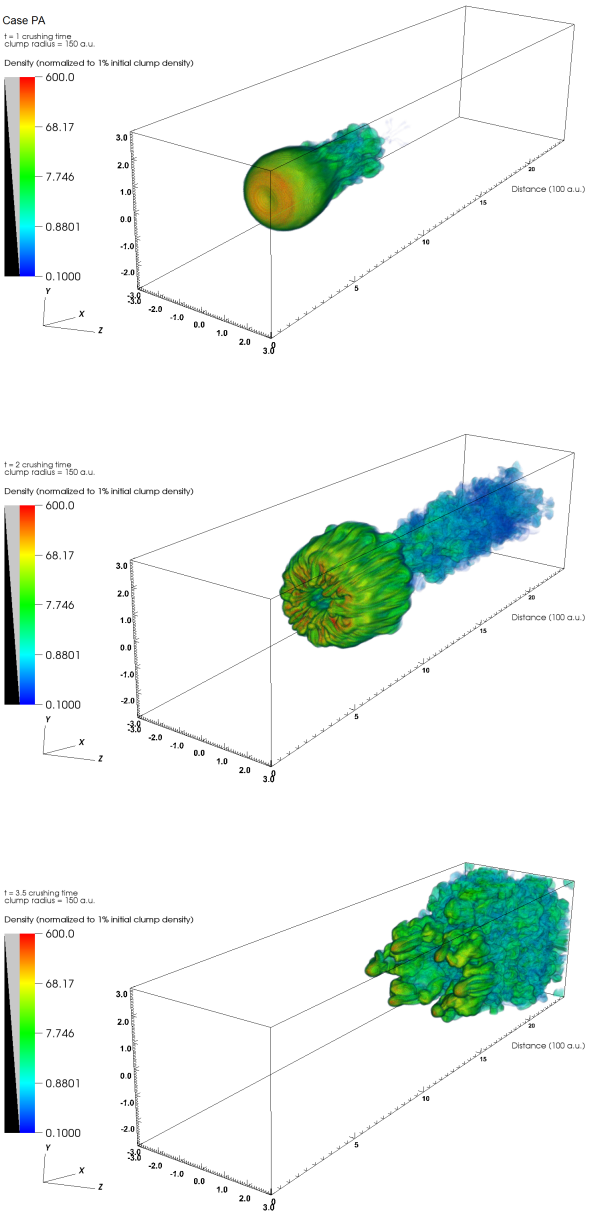

Figure 4: Case of poloidal field only, aligned with shock propagation direction (coded PA). Evolution of clump material at 1, 2 and 3.5 clump crushing times. The color indicates clump material concentration, normalized by initial value.

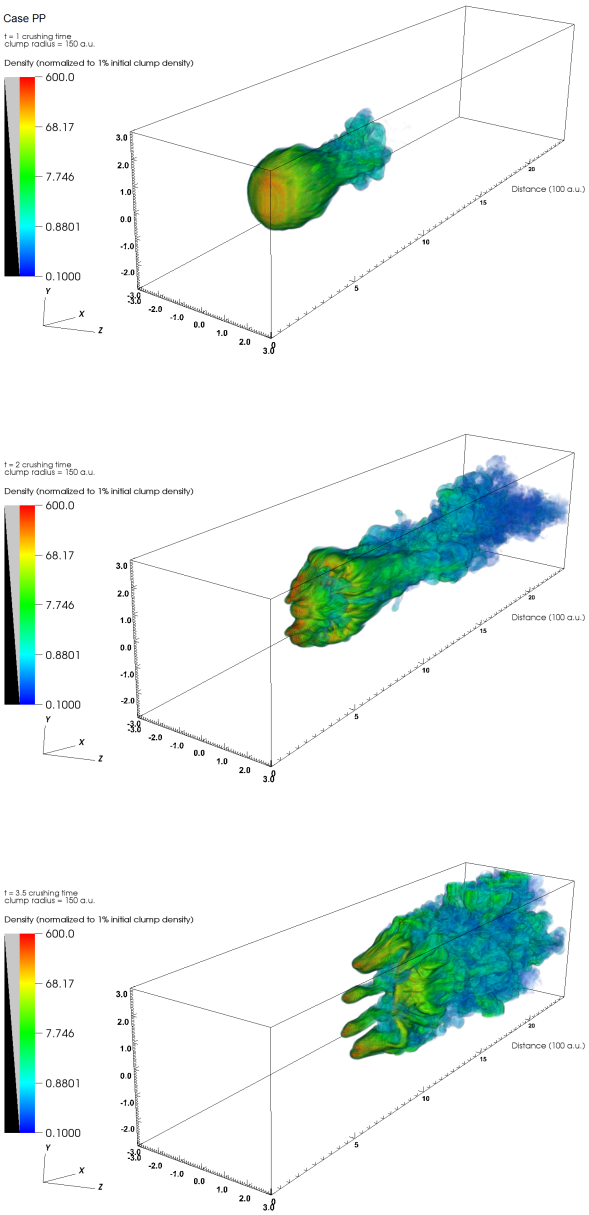

Figure 5: Case of poloidal field only, perpendicular to shock propagation direction (coded PP). Evolution of clump material at 1, 2 and 3.5 clump crushing times. The color indicates clump material concentration, normalized by initial value.

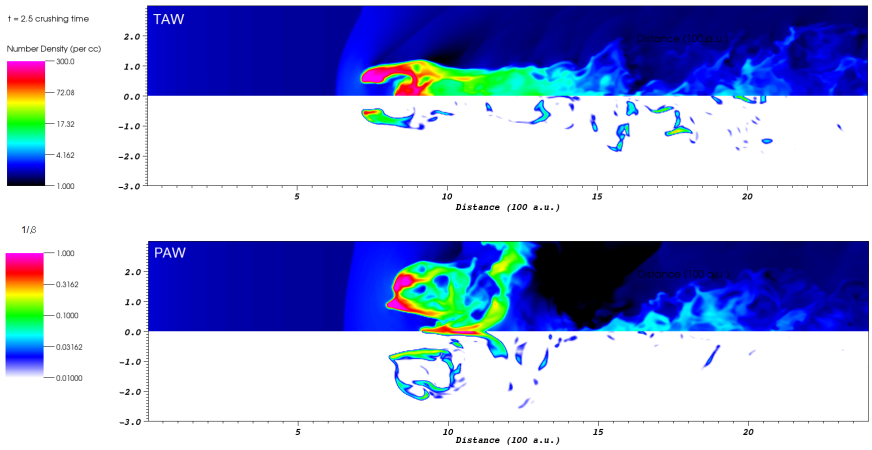

Figure 6: Snapshot of shocked clumps cutthrough the center of the domain, at $t = 2.5\tau_{cc}$, for the TAW and PAW cases. The upper panel corresponds to the density, the lower panel corresponds to $1/\beta$.

the TA case, the material is mostly compressed into a cone, leading to very limited downstream turbulent region. In both TP and PP cases, the turbulence fills a much larger region, but still does extend across the entire box downstream. In the PA case, because of the expanding "ring" feature, the downstream turbulence fills the entire box cross section. The aftermath of the shocked clumps is also vastly different: The TA case forms a "nose cone" feature at the end, while in the other three cases, smaller magnetized "clumplets" are formed with different spatial distributions.

Magnetic fields can be important in suppressing the instabilities associated with shocked clumps. According to Jones' early paper [1], the condition for the magnetic field to suppress the KH instability is that $\beta < 1$ for the boundary flows. The condition for the magnetic field to suppress the Rayleigh-Taylor instability is that $\beta < \xi/M = 10$. For both strong and weak field cases presented in our paper, the β at the boundary flows has a value between 1 and 10. Therefore the KH instability is present in all of our cases, shredding the clump boundary flows and converting them into downstream turbulence. We use "TAW" and "PAW" to denote cases with the same as the "TA" and "PA" cases before, but with a higher magnetic *beta*: $\beta_{avg} = 1$. From Fig.6, we can see that even for the weak self-contained field cases, the Rayleigh-Taylor instability is suppressed. In Fig.6, we map the density and β (presented by $1/\beta$) for TAW and PAW cases. We observe that the shocked clump material develops a streamlined shape in both cases. The region where density is concentrated has $1/\beta > 0.1$.

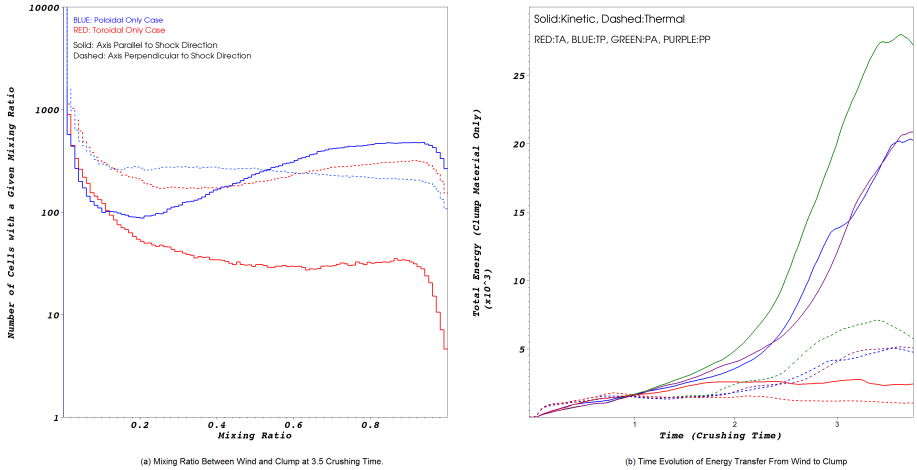

(a) Mixing Ratio Between Wind and Clump at 3.5 Crushing Time.

(b) Time Evolution of Energy Transfer From Wind to Clump

Figure 7: (a) Mixing ratio between wind and clump material at $3.5\tau_{cc}$ of the presented simulations. (b) Time evolution of kinetic and thermal energy contained in the clump material in computation units, indicating how much energy has transferred from wind into clump.

5. Mixing between clump and wind

Fig.7(a) shows the mixing ratio at $3.5\tau_{cc}$ of different cases presented in the previous section. The mixing ratio is defined by the following equation in a single cell:

$$\eta = \frac{2min(n_c, n_w)}{n_c + n_w} \tag{12}$$

where n_c and n_w denote the clump and wind number densities, respectively. This definition shows that $\eta = 1$ means perfect mixing: there is equal number of clump and wind particles in the cell, while $\eta = 0$ means no mixing at all. The PA configuration has the highest mixing ratio in the four studied cases. The PP and TP cases have similar intermediate mixing ratios, and the TA has the lowest mixing ratio. The mixing ratio partially depends on the efficacy of turbulent mixing downstream.

By looking at the 3D images of the previous section, we can identify the downstream turbulence of the TA and PA cases as the least and most volume filling respectively. The mixing ratio comparison also agrees with our intuition that the more the aerodynamic resistance provided by the field configuration, the less the mixing. This is borne out by the 4 cases: the toroidal aligned case has its field lines entirely aligned with the incoming shock plane; the two perpendicular cases have most of the field lines aligned with the shock plane, but there are also components that are along the shock direction; the PA case has most of its field aligned with the shock normal.

Fig.7(b) shows the time evolution of kinetic and thermal energy contained in the clump material. Here we see similar behavior as in the mixing ratio plot:

the more the initial field lines are perpendicular to the shock normal, the less energy transferred from wind to clump.

6. Conclusion

Using 3-D AstroBEAR MHD simulations, we have demonstrated that shocked clumps with self-contained internal magnetic fields show a rich, but qualitatively understandable behavior not seen in previous simulations of shock-clump interactions which employed ordered background fields extending through both the clump and the ambient gas.

We find that the post-shock evolution depends strongly on internal field morphology. The energy transfer from wind to magnetic field and the mixing of wind and clump material also depend on the field geometry. In general, the more perpendicular the clump magnetic field is to the direction of shock propagation, the more aerodynamic resistance the field provides, and the less the mixing and energy transfer occurs.

These simulations offer principles that may help understand the morphology evolution of structures in clumpy astrophysical environments. Future studies could include more diverse field geometries and more realistic treatments of processes such as thermal conduction and resistivity.

7. Acknowledgments

This work is supported by U.S Department of Energy, National Science Foundation, Space Telescope Science Institute and Laboratory for Laser Energetics. The authors would also like to thank Jonathan Carrol and Martin Huarte-Espinosa for useful discussions and suggestions.

[1] T.W. Jones, D. Ryu, I.L. Tregillis, The Magnetohydrodynamics of Supersonic Gas Clouds: MHD Cosmic Bullets and Wind-swept Clumps, Astrophys J. 473 (1996) 365-382

[2] M.S. Shin, J.M. Stone, G.F. Snyder, The Magnetohydrodynamics of Shock-Cloud Interaction in Three Dimensions, Astrophys J. 680 (2008) 336-348

[3] R.I. Klein, C.F. McKee, P. Colella, , Astrophys J. 420(1994) 213

[4] A.Y. Poludnenko, A. Frank, E.G. Blackman, , Astrophys J. 576(2002) 832

[5] J.M. Stone, M.L. Norman, , Astrophys J. 390(1992) 17

[6] G. Mellema, J.D. Kurk, H.J.A Rottgering, , aa 395(2002) 13

[7] P.C. Fragile, S.D. Murray, P. Anninos, van W. Breugel, , Astrophys J. 604(2004) 74

[8] F. Nakamura, C.F. McKee, R.I. Klein, R.T. Fisher, , Astrophys J. 164(2006) 477

[9] F. Miniati, D. Ryu, A. Ferrara, T.W. Jones, , Astrophys J. 510(1999) 726

[10] R.I. Klein, D.T. Woods, , Astrophys J. 497(1998) 777

[11] J.M. Pittard, S.A.E.G. Falle, T.W. Hartquist, J.E. Dyson, , MNRAS 394(2008) 1351

[12] P.C. Fragile, P. Anninos, K. Gustafson, S.D. Murray, Magnetohydrodynamic Simulations of Shock Interactions with Radiative Clouds, Astrophys J. 619 (2005) 327-339

[13] S. Orlando, F. Bocchino, F. Reale, G. Peres, P. Pagano, The Importance of Magnetic-Field-Oriented Thermal Conduction in the Interaction of SNR Shocks with Interstellar Clouds, Astrophys J. 678 (2008), 274-286

[14] Shule Li, A. Frank, E. Blackman, Consequences of Magnetic Field Structure for Heat Transport in Magnetohydrodynamics, Astrophys J. 748 (2012), 24-37

[15] A.J. Cunningham, A. Frank, R. Varnière, S. Mitran, T.W. Jones, , Astrophys J. 182(2009) 519

[16] J. Carroll, A. Frank, , Comput. J. (2012) submitted

[17] A. Dalgarno, R.A. McCray, Heating and Ionization of HI Regions, Annu Rev Astron Astrophys. 10 (1972), 375-426

[18] A. Frank, D. Ryu, T.W. Jones, A. Noriega-Crespo, Effects of Cooling on the Propagation of Magnetized Jets, Astrophys J. 494 (1998), 79-83

[19] K.R. Lind, D.G. Payne, D.L. Meier, R.D. Blandford, Numerical simulations of magnetized jets, Astrophys J. 344 (1989), 89-103